AN INTERFACE ELEMENT FOR GLOBAL/LOCAL AND SUBSTRUCTURING ANALYSIS

Jerrold M. Housner†
NASA Langley Research Center
Mohammad A. Aminpour*
Old Dominion University
Carlos G. Dávila**
National Research Council Associate
John E. Schiermeier***
The MacNeal-Schwendler Corporation
W. Jefferson Stroud‡, Jonathan B. Ransom‡, and Ronnie E. Gillian‡
NASA Langley Research Center

Abstract

NASA and the MacNeal Schwendler Corporation have entered into a cooperative agreement to further the development of Interface Technology for finite element modeling. This new technology enables incompatibly meshed models to be accurately joined together even when their grid points do not coincide. Until recently, this technology was being developed solely by NASA. To improve technology transfer and to ensure relevancy of NASA developments in this area, NASA and MSC will work together to extend the capability in an experimental version of MSC/NASTRAN. This paper describes the Interface Technology, demonstrates its capabilities and value, and reviews the activity of the NASA/MSC joint venture.

---

† Head, Computational Structures Branch, Mail Stop 240, Hampton, VA, 23681.

* Associate Professor, Aerospace Engineering Department, Norfolk, VA, 23529.

** Senior Scientist, Currently at Analytical Services and Materials, Inc., 107 Research Drive, Hampton, VA, 23666.

*** Senior Development Engineer, 815 Colorado Boulevard, Los Angeles, CA, 90041.

‡ Aerospace Engineers, Computational Structures Branch, Mail Stop 240, Hampton, VA, 23681.

Introduction

Reliable predictions of detailed stress states are needed during the design of aerospace structures in order to understand and predict the behavior and failure mechanisms of such structures. While the finite element method can provide accurate detailed stress predictions of structures with complex geometries, fine mesh discretizations of the structures are needed in the vicinity of a stress or strain concentration. The resulting finite element models generally contain both fine and coarse finite element meshes. Obtaining fine finite element meshes in certain regions and coarse meshes in other regions usually requires transition modeling that is tedious, costly, and time consuming. In addition, the transition modeling usually results in distorted elements which introduce errors.

Methods which do not require nodal compatibility on substructure boundaries (edges) provide modeling flexibility and eliminate the need for complex mesh transitioning. Several such coupled methods have been developed over the years. Some of these methods have used multipoint constraints along the common subdomain boundaries. These methods have typically had difficulty in maintaining solution accuracy, particularly near the common substructure boundaries[1–2]. In reference 3 an effective method was developed in which an independent function is used to connect two substructures. In that work, three formulations for coupling independently modeled substructures were developed and studied. The hybrid variational formulation was shown to be the most robust and accurate of the three formulations examined. This formulation preserves solution accuracy (of displacements and stresses) across the common substructure interfaces. Additional applications which illustrate the formulation and the coupling method have also been reported in reference 4. The hybrid variational formulation has been recast into the form of an interface finite element, as reported in reference 5, which extends its capability to multiple substructures, multiple and possibly nested interfaces, and curved interfaces. Additional applications which illustrate this extension were reported in reference 6. The interface element allows the independent modeling of different regions or components without concern for the nodal compatibility between the finite element models.

For the engineer who is applying the interface element, the models of the substructures have to be generated in the usual manner (e.g., with MSC/PATRAN), and, in addition, the engineer has to provide data for the location of the interface describing how the substructures are connected to each other. Although the modeling of substructures is much simpler than transition modeling, the time saving may not be so much as to warrant the use of the method for a single modeling effort. However, substantial time saving will occur during a parametric study, where the local model of a critical region (e.g., a hole or a crack) has to be changed many times while keeping the other models unchanged.

As will be discussed later, the interface element may also be used to couple independently modeled intersecting substructures as shown in Figure 2. In this application of the interface element some minor remeshing is required (as shown in Figure 3) in order to transform the problem of intersecting

substructures to that of connecting substructures along their boundaries. In this case substantial time saving will occur during a parametric study, where the relative location of the substructures has to be changed many times while keeping the models unchanged.

It is emphasized here that the interface element does not improve the performance of the finite elements used in the analysis and therefore does not improve the quality of the results attainable by a particular element. However, by eliminating or reducing transition modeling, the introduction of distorted elements into the finite element model is limited to what is necessary to represent the geometry of the component. Therefore, no additional errors associated with mesh distortion are introduced. The elimination of unnecessary element distortion errors allows the use of coarser meshes, and, therefore, the same qualitative results may be obtained with a smaller number of degrees of freedom.

In this paper the mathematical description of the interface element, together with possible extensions, is presented first. Then, several representative global/local and substructuring examples are presented to demonstrate the capabilities of the method. Finally, the implementation aspects of the technology into MSC/NASTRAN are discussed.

Mathematical Description of the Interface Element

In this section the formulation of a typical interface element is presented. The implementation is not restricted to one interface element; an arbitrary number of interface elements may be used in a single analysis.

Consider, for example, the domain shown in Figure 1 and modeled as three independently discretized substructures, $\Omega_1, \Omega_2, \Omega_3$. The depiction of three substructures is for discussion purposes only; the element formulation and implementation are generally applicable to an arbitrary number of independently discretized substructures. The generally curved interface element path, S_I, is discretized with a mesh of evenly spaced pseudo-nodes (open circles in Figure 1) which need not be coincident with the interface nodes (filled circles in Figure 1) of any of the substructures. That is, the discretization of the interface path is independent of the discretization of the connected substructures. The initial assumption is that along an interface element the displacement vector, $\mathbf{v}$, is given by

$$\mathbf{v} = \mathbf{T}\mathbf{q}_s \tag{1}$$

where $\mathbf{T}$ is a matrix of interpolating functions and $\mathbf{q}_s$ is a vector of generalized displacements associated with the pseudo-nodes. The interpolation matrix $\mathbf{T}$ is formed by passing a cubic spline through the evenly spaced pseudo-nodes.

In the hybrid variational formulation, the total potential energy equation is modified to include an integral form for the compatibility between the interface and the subdomains and for the three independently modeled substructures shown in Figure 1 is given by

$$\Pi = \Pi_{\Omega_1} + \Pi_{\Omega_2} + \Pi_{\Omega_3} + \int_S \boldsymbol{\lambda}_1^{\mathrm{T}} (\mathbf{v} - \mathbf{u}_1)\, ds + \int_S \boldsymbol{\lambda}_2^{\mathrm{T}} (\mathbf{v} - \mathbf{u}_2)\, ds + \int_S \boldsymbol{\lambda}_3^{\mathrm{T}} (\mathbf{v} - \mathbf{u}_3)\, ds \tag{2}$$

where Π_{Ω_j} is the total potential energy, $\boldsymbol{\lambda}_j$ is a vector of Lagrange multipliers, and $\mathbf{u}_j$ is the displacement field vector along the interface for subdomain j ($j = 1, 2, 3$). The constraint integrals are added to the functional to enforce the continuity, in the variational sense, of displacements across the interface. Equation 2 corresponds to the "double layer interface" or "frame" method of the hybrid variational principle[7] and has in the past been used primarily to enforce compatibility between adjacent elements that have incompatible assumed displacement shape functions within the context of a nodally compatible finite element model[8–11]. Herein, however, the variational statement in equation 2 is utilized to enforce compatibility between nodally incompatible finite element models.

Assuming that the displacement boundary conditions are satisfied, the stationary condition for the modified total potential energy for arbitrary $\mathbf{u}_j$ in the subdomains, arbitrary $\mathbf{v}$ on the interface, S, and arbitrary $\boldsymbol{\lambda}_j$ on the interface parts of the subdomains, reveals 1) that the Lagrange multipliers $\boldsymbol{\lambda}_j$ represent the tractions on the interface for subdomain j, 2) that the sum of these tractions across the interface is zero (i.e., equilibrium is maintained, in the variational sense, across the interface), and 3) that the displacement field on the interface for subdomain j is equal to the assumed displacement field, v, along the interface (i.e., displacement continuity is maintained, in the variational sense, across the interface).

In the finite element discretization, the displacements, $\mathbf{u}_j$, and the Lagrange multipliers, $\boldsymbol{\lambda}_j$, are independently approximated for each element along the interface, and the displacement field, $\mathbf{v}$, is approximated on the interface, S, as discussed previously. The displacements, $\mathbf{u}_j$, along the interface are expressed in terms of unknown nodal displacements, $\mathbf{q}_j^i$ (the superscript i refers to the interface nodes of the substructure), as $\mathbf{u}_j = \mathbf{N}_j \mathbf{q}_j^i$, and the Lagrange multipliers, $\boldsymbol{\lambda}_j$, are expressed in terms of unknown coefficients, $\boldsymbol{\alpha}_j$, as $\boldsymbol{\lambda}_j = \mathbf{R}_j \boldsymbol{\alpha}_j$, where $\mathbf{N}_j$ and $\mathbf{R}_j$ are matrices of interpolating functions. The interpolating functions in the matrix, $\mathbf{R}_j$, are taken to be constant parameters for linear elements and linear functions for quadratic elements. With these assumptions, equation 2 may be rewritten as

$$\Pi = \Pi_{\Omega_1} + \Pi_{\Omega_2} + \Pi_{\Omega_3} + \boldsymbol{\alpha}_1^{\mathrm{T}} \mathbf{M}_1^{\mathrm{T}} \mathbf{q}_1^i + \boldsymbol{\alpha}_2^{\mathrm{T}} \mathbf{M}_2^{\mathrm{T}} \mathbf{q}_2^i + \boldsymbol{\alpha}_3^{\mathrm{T}} \mathbf{M}_3^{\mathrm{T}} \mathbf{q}_3^i + \boldsymbol{\alpha}_1^{\mathrm{T}} \mathbf{G}_1^{\mathrm{T}} \mathbf{q}_s + \boldsymbol{\alpha}_2^{\mathrm{T}} \mathbf{G}_2^{\mathrm{T}} \mathbf{q}_s + \boldsymbol{\alpha}_3^{\mathrm{T}} \mathbf{G}_3^{\mathrm{T}} \mathbf{q}_s \qquad (3)$$

where $\mathbf{M}_j$ and $\mathbf{G}_j$ are integrals along the interface defined in terms of $\mathbf{R}_j$, $\mathbf{N}_j$, and $\mathbf{T}$ as

$$\mathbf{M}_j = -\int_S \mathbf{N}_j^{\mathrm{T}} \mathbf{R}_j \, ds \quad \text{and} \quad \mathbf{G}_j = \int_S \mathbf{T}^{\mathrm{T}} \mathbf{R}_j \, ds \quad ; \quad j = 1, 2, 3 \qquad (4)$$

Taking the first variation of the modified total potential energy with respect to the independent variables

$(\mathbf{q}_j^i,\ \mathbf{q}_j^o,\ \mathbf{q}_s,\ \boldsymbol{\alpha}_j,\ j=1,2,3)$ and setting it to zero yields the system of equations

$$\begin{bmatrix} \mathbf{K}_1^{ii} & \mathbf{K}_1^{io} & 0 & 0 & 0 & 0 & 0 & \mathbf{M}_1 & 0 & 0 \\ \mathbf{K}_1^{oi} & \mathbf{K}_1^{oo} & 0 & 0 & 0 & 0 & 0 & 0 & 0 & 0 \\ 0 & 0 & \mathbf{K}_2^{ii} & \mathbf{K}_2^{io} & 0 & 0 & 0 & 0 & \mathbf{M}_2 & 0 \\ 0 & 0 & \mathbf{K}_2^{oi} & \mathbf{K}_2^{oo} & 0 & 0 & 0 & 0 & 0 & 0 \\ 0 & 0 & 0 & 0 & \mathbf{K}_3^{ii} & \mathbf{K}_3^{io} & 0 & 0 & 0 & \mathbf{M}_3 \\ 0 & 0 & 0 & 0 & \mathbf{K}_3^{oi} & \mathbf{K}_3^{oo} & 0 & 0 & 0 & 0 \\ 0 & 0 & 0 & 0 & 0 & 0 & 0 & \mathbf{G}_1 & \mathbf{G}_2 & \mathbf{G}_3 \\ \mathbf{M}_1^{\mathrm{T}} & 0 & 0 & 0 & 0 & 0 & \mathbf{G}_1^{\mathrm{T}} & 0 & 0 & 0 \\ 0 & 0 & \mathbf{M}_2^{\mathrm{T}} & 0 & 0 & 0 & \mathbf{G}_2^{\mathrm{T}} & 0 & 0 & 0 \\ 0 & 0 & 0 & 0 & \mathbf{M}_3^{\mathrm{T}} & 0 & \mathbf{G}_3^{\mathrm{T}} & 0 & 0 & 0 \end{bmatrix} \begin{bmatrix} \mathbf{q}_1^i \\ \mathbf{q}_1^o \\ \mathbf{q}_2^i \\ \mathbf{q}_2^o \\ \mathbf{q}_3^i \\ \mathbf{q}_3^o \\ \mathbf{q}_s \\ \boldsymbol{\alpha}_1 \\ \boldsymbol{\alpha}_2 \\ \boldsymbol{\alpha}_3 \end{bmatrix} = \begin{bmatrix} \mathbf{f}_1^i \\ \mathbf{f}_1^o \\ \mathbf{f}_2^i \\ \mathbf{f}_2^o \\ \mathbf{f}_3^i \\ \mathbf{f}_3^o \\ 0 \\ 0 \\ 0 \\ 0 \end{bmatrix} \tag{5}$$

where the superscript o refers to non-interface nodes of the substructures; and $\mathbf{q}_j$ is the generalized displacement vector, $\mathbf{f}_j$ is the external force vector, and $\mathbf{K}_j$ is the stiffness matrix associated with subdomain j. The system of equations given by equation 5 is symmetric and sparse but, not banded and not positive definite. Herein, a sparse solver with out-of-core capability for symmetric, non-positive definite systems developed by Boeing Computer Services[12] is used for this class of problems.

An examination of equation 5 reveals that the assembled stiffness matrices of the substructures are uncoupled in a block diagonal form and are coupled through the matrices $\mathbf{M}_j$ and $\mathbf{G}_j$. Furthermore, the form of equation 5 suggests that the following may be identified as the "stiffness" matrix and the vector of generalized nodal displacements and the Lagrange multiplier paramcters for the interface element

$$\begin{bmatrix} 0 & 0 & 0 & 0 & \mathbf{M}_1 & 0 & 0 \\ 0 & 0 & 0 & 0 & 0 & \mathbf{M}_2 & 0 \\ 0 & 0 & 0 & 0 & 0 & 0 & \mathbf{M}_3 \\ 0 & 0 & 0 & 0 & \mathbf{G}_1 & \mathbf{G}_2 & \mathbf{G}_3 \\ \mathbf{M}_1^{\mathrm{T}} & 0 & 0 & \mathbf{G}_1^{\mathrm{T}} & 0 & 0 & 0 \\ 0 & \mathbf{M}_2^{\mathrm{T}} & 0 & \mathbf{G}_2^{\mathrm{T}} & 0 & 0 & 0 \\ 0 & 0 & \mathbf{M}_3^{\mathrm{T}} & \mathbf{G}_3^{\mathrm{T}} & 0 & 0 & 0 \end{bmatrix}, \begin{bmatrix} \mathbf{q}_1^i \\ \mathbf{q}_2^i \\ \mathbf{q}_3^i \\ \mathbf{q}_s \\ \boldsymbol{\alpha}_1 \\ \boldsymbol{\alpha}_2 \\ \boldsymbol{\alpha}_3 \end{bmatrix} \tag{6}$$

Herein, the above formulation is applied to general 2D curvilinear shell structures. However, the formulation is general and may be specialized for coupling of 3D finite element models. This extension requires an accurate description of the common surface between 3D models. Surface splines may be used to accomplish this. The surface description which has to be obtained from the nodes on the surface of the 3D models must be smooth. Otherwise, the solution will be inaccurate, particularly near the common surface, due to the roughness of the surface description. Work is underway for this extension of the interface technology presented in this paper.

Enhancements of the Interface Element

In the introduction and in the previous section it was said that the interface element could be used to connect independently modeled substructures along their boundaries (edges). The interface element may also be used to permit coupling between independently modeled intersecting substructures as shown if Figure 2. In this case the components of a built-up structure can be modeled independently

and then connected to each other. The finite element meshes need not be nodally compatible, and the boundary nodes of one component (e.g., the stiffener) may cross the faces of the elements of the other component (e.g., the skin). In reference 13, a "cross-surface interface element" was developed to couple independently modeled intersecting substructures. In that work the integrals in equation 4 of the previous section translate into line integrals along the common interface between substructures over the surface of the elements whose faces are crossed. This makes the formulation more complicated because now all the nodes of the elements whose faces are crossed enter into the formulation, and a good mathematical description of the intersecting line needs to be computed (see reference 13). Furthermore, intersecting the faces of the elements of one component (e.g., the skin) with the edges of the elements of another component (e.g., the stiffener) is equivalent to applying a line load over the surface (i.e., in the interior) of the elements whose faces are crossed. As was shown in reference 13, this method can produce inaccurate results in some extreme cases. These inaccuracies, however, are not a direct result of the formulation, but rather are a result of the inability of the elements whose faces are crossed to accurately deal with loads in their interior. This inability to deal with interior loads is true of nearly all finite elements because the interior loads are translated into nodal loads, and the distribution of forces and moments will not be correct over the element.

A remedy for this inability of finite elements to accurately represent interior loads is to split the elements whose faces are crossed (along the line of intersection) into several elements as necessary as shown in Figure 3. In this way, the problem of finite elements having to deal with interior loads is eliminated and the load transfer between different components takes place through element edges. Although, this splitting of elements produces some distorted elements, the number of distorted elements is small and their location is limited to a small region adjacent to the line of intersection.

Once the elements whose faces are crossed are properly split into several elements, the coupling of the independently modeled components reduces to coupling of substructures with nodal incompatibility along their common interface as presented in the previous section. This method is referred to herein as the "cross-split method". The cross-split method may be considered more of an implementation and bookkeeping issue than a mathematical issue. The program has to keep track of additional nodes and elements that are generated by splitting of the elements whose faces are crossed.

Applications

The interface element formulation described in this paper has been used to analyze four representative global/local and substructuring examples. An isotropic plate with a circular hole subjected to uniform tension is presented first. This example demonstrates the accuracy and the use of the interface element in studying the effect of details in structural design, such as hole configurations. The potential use of the interface element in structural analysis is next demonstrated on more complicated examples.

These examples include a free-edge stress problem and a representative composite laminate fuselage crown panel. The final example is a fuselage side panel with a circular cutout and two frames. This last example demonstrates the use of the cross-split method in independent component modeling of built-up structures.

Tension-Loaded Plate with a Central Circular Hole

A plate which has a central circular hole of radius R_0 and which is loaded in uniform tension (shown in Figure 4) is an ideal example problem with which to verify the global/local capability of the interface element since an exact solution is available. One quarter of the plate was modeled in the coupled analysis. A refined model was used in the near-field subdomain (*i.e.*, the local subdomain, near the hole), and a coarse, much less refined, model was used in the far-field subdomain (*i.e.*, the global subdomain, away from the hole). The global and local finite element models are shown in Figure 4. The interface is located at $0.4R_0$ away from the edge of the hole to demonstrate the robustness of the method when the interface is placed in a region of high stress gradient.

The exact elasticity solution for an infinite plate which has a central circular hole and which is loaded in uniform tension shows that the stress concentration factor, K_t, is equal to 3.0 at the edge of the hole[14]. The stress concentration factor K_t is defined as the ratio of the maximum longitudinal stress resultant $(N_x)_{max}$ to the uniform far-field longitudinal stress resultant $(N_x)_0$.

The distributions of the hoop stress resultant N_θ along the $\theta = 0$ line (along the x-axis) and along the $\theta = \pi/2$ line (along the y-axis) normalized by the uniform far-field longitudinal stress resultant, $(N_x)_0$, are shown in Figure 4 as a function of the distance, r, from the plate center normalized by the hole radius, R_0. The stress distributions predicted by the coupled analysis are in excellent agreement with the elasticity solution[14].

Tension-Loaded Composite Laminate

A composite laminate plate shown in Figure 5 subjected to uniform tension demonstrates the use of the interface element with different types of finite elements. In this application, the interface element is used in conjunction with 2D-3D transition elements to couple the two- and three-dimensional idealizations in order to reduce the modeling effort and the number of degrees of freedom required in the analysis. Solutions are available in the literature for the configuration of Figure 5, referred to as the free-edge stress problem[15]. The laminate is a 4-ply [0/90]s tensile coupon under uniform axial strain, ϵ_x. The ply thickness is h, the width is 16h, and the length is 48h. The ply properties are 20,000 ksi for the longitudinal Young's modulus, 2100 ksi for the transverse Young's moduli, 850 ksi for the shear moduli, and 0.21 for the three independent Poisson's ratios.

The 3D solid element used in the analysis is a 20-node, isoparametric, serendipity element[16] with three degrees of freedom at each node (i.e., three displacements). The 2D shell element is the 9-node

ANS (Assumed Natural Strain) element[17] with 5 degrees freedom (i.e., three displacements and two rotations). The 2D-3D transition elements are 15-node and 12-node elements[18] and make use of kinematic constraints to enforce compatibility between the shell and 3D elements. These elements may be used to connect one shell element to many layers of solid elements. The transition elements have three translational degrees of freedom at each node. Each node within the transition element that is connected to a shell element has two additional rotational degrees of freedom.

When the laminate is subjected to a uniform tensile strain, ϵ_x, each of the x = constant planes will deform in the same manner. Therefore, the problem does not require a 3D analysis. However, such an analysis has been reported[19] to illustrate the use of 2D-3D transition elements. Taking advantage of the symmetry in the problem, only half of the laminate was modeled. In that work, the 3D discretization of the laminate propagates into the rest of the model (where such refinement is not needed), thus creating both a large 3D model and a larger-than-necessary 2D model. The size of the 2D model (622 active degrees of freedom[19]) can be reduced with the use of the interface elements described herein.

The finite element models used in the current, coupled analysis are shown in Figure 5 (denoted Coupled Model I). The shaded region represents the local finite element model with the 3D elements indicated by the darker shading and the 2D-3D transition elements indicated by the lighter shading. The remainder of the laminate (the 2D substructure) is modeled with the 9-node ANS shell elements and has only 198 degrees of freedom (about one third the size of the 2D model previously reported[19]). Compatibility between the shell and 2D-3D transition elements is enforced using interface elements (thick hatched lines in Figure 5). Two analyses have been performed: one with the same discretization in the local region as that reported in reference 19 (denoted Local Model I in Figure 6) and a second with greater local refinement and with the mesh graded towards the free edge (denoted Local Model II in Figure 6). Both analyses use the same 2D mesh shown in Figure 5. This demonstrates the modeling flexibility permitted by use of the interface element since changes in the modeling of the local 3D finite element model do not affect the discretization of the coarser 2D finite element model. Additionally, had a nodally compatible 2D model been generated in the second case, it would have required far more degrees of freedom in order to ensure that the shell element aspect ratios remained within a reasonable range near and along the free edge (y = b) of the model.

Ply interface stresses were obtained by linearly interpolating the Gauss point data of the elements above and below the 0/90 interface. The σ_z and τ_{yz} distributions along the 0/90 interface at the midlength (x = 0) normalized by the uniform far-field strain, $\epsilon_x \text{x} 10^6$, are shown in Figure 6. The open circles represent the solution obtained from the coupled analysis with the less refined 3D model (Local Model I). The filled circles represent the solution obtained from the coupled analysis with the more refined, graded 3D model (Local Model II). The solution obtained from the first analysis, with the coarser 3D model (open circles in the figures), is in excellent agreement with the reference single model

solution from reference 18. In addition, a qualitative comparison reveals that the coupled solution is in overall good agreement with the theoretical solution[15] (solid lines in the figures). The solution obtained from the second analysis (filled circles in the figures) delineates the gradient at the free edge better than the solution obtained with the less refined local model. Additional refinement is necessary at the free edge to further delineate the gradient; however, the purpose of this example was to demonstrate the interface element while comparing with the previous 2D-3D analysis[19]. Thus no further refinement of the 3D model was pursued.

Composite Crown Panel

A composite laminated fuselage crown panel form The Boeing Company, shown in Figure 7, is analyzed next. The panel is curved with a radius of 122 in., is 64 in. long and has a cord length of 68 in. The panel has five hat-stiffener stringers and three J-frames and is nearly, but not completely, symmetric due to the J-frames and the unsymmetric material lay-up. A hydrostatic pressure load is applied and repeating unit boundary conditions are assumed. The objective of this analysis is to provide a description of the stress field in the neighborhood of a typical mouse hole (opening where a J-frame crosses over a hat-stiffener). A more detailed geometry of a typical mouse hole is also shown in the figure. In this region there is a small gap between the flange of the hat-stiffener and the flange of the J-frame. A test, designed to simulate the hydrostatic pressure load on the panel, revealed that a delamination may develop between the skin and the flange of the J-frame along this gap at the mouse hole area[20]. Figure 8 shows a typical finite element model of a mouse hole region. This model was developed using the MSC/PATRAN graphics software system by other analysts at NASA Langley to perform a detailed stress analysis of a mouse hole region. As shown in the figure, the region in the immediate vicinity of the mouse hole was modeled with a fine finite element mesh while the region away from the mouse hole was modeled with a coarser finite element mesh. Transition modeling was used to connect the fine finite element model to the coarser finite element model and can be seen to produce distorted and badly shaped quadrilateral elements. As mentioned earlier, these elements do not produce accurate and reliable results in regions of high stress gradients. Ironically this is where accurate stresses are needed to make a reliable assessment of the failure modes of the structure. Also, if the entire panel is to be analyzed, the rest of the panel would need to be modeled with a still coarser refinement (in order to keep the problem size manageable) which would require a second level of transition modeling.

In contrast to transition modeling, the modeling of the panel with the interface elements is relatively simple. There is no need for distorted elements except what is needed to represent the geometry of the structure, and, therefore, the finite element meshes can be constructed as regularly as possible. To analyze this panel, three separate finite element meshes were developed as shown in Figure 9. The immediate region of interest was modeled with a highly refined finite element mesh (the sublocal model).

The region in close proximity to the region of interest was modeled with a coarser finite element mesh (the local model) and the rest of the panel was modeled with the coarsest mesh (the global model). The sublocal model is connected to the local model with eight interface elements and the local model is connected to the global model with twenty interface elements for a total of twenty eight interface elements in the model. The number of interfaces needed to connect the models together is simply the number of boundaries (edges) that connect one region or substructure to another. The sublocal region was modeled with eight MSC/PATRAN patches. If further refinement of the sublocal model is needed (for further investigation or indicated by some error indicators) only those eight patches forming the sublocal model need to be refined. No changes to the other two models (i.e., the local and global models) are required. In contrast, transition modeling would typically require substantial remeshing of the panel. This modeling flexibility may become very important in the design process by permitting very coarse meshes of fixed, global features and very fine, interchangeable meshes of different local features. In the present application, for example, various mouse hole geometries could be analyzed by simply changing the mesh for the sublocal model.

Figure 10 shows the three substructures (which make up the entire structure) connected together. The relative mesh sizes of different levels of refinement can be seen in this figure. The local model is highly refined as compared with the global model, and the sublocal model is, in turn, highly refined as compared to the local model. The deformation contours as seen from the panel interior – the skin, the hat-stiffeners, and the J-frames – are shown in Figure 11a. The deformation contours as seen from the panel exterior are shown in Figure 11b. It is seen that the pressure pillowing in the interior four bays have a greater magnitude than in the exterior four bays as expected. The deformation pattern is nearly but not totally symmetric. This is expected since, as mentioned earlier, the geometry of the panel, due to the presence of the J-frames and the material lay-up, is not totally symmetric.

Figure 12 shows the hoop stress resultant contours on the panel. Globally, there is little variation in the hoop stress resultant. However, a closer look at the sublocal region reveals that there is a strong stress concentration at the mouse hole area in the gap between the hat-stiffener flange and the J-frame flange. This is in agreement with the test results which have shown that a delamination may develop between the skin and the flange of the J-frame along the gap at the mouse hole area[20].

Figure 13 shows the effect of different levels of discretization in capturing the stress gradients. Figure 13a shows the hoop stress distribution for the global model (the coarsest finite element mesh) at a mouse hole along the gap between a hat-stiffener flange and a J-frame flange. This coarse mesh is simply not capable of capturing the stress gradients in this region. Figure 13b shows the hoop stress distribution for the local model (the moderately refined finite element mesh) at the mouse hole area along the gap between a hat-stiffener flange and a J-frame flange. Although the local model better captures the stress concentration in this region, it is still not fine enough to represent accurately the stress gradients in this

region. Finally, Figure 13c shows the hoop stress distribution for the sublocal model (the highly refined finite element mesh) at a mouse hole area along the gap between a hat-stiffener flange and a J-frame flange. The sublocal model captures the stress gradients in this region much better than either the global or local models.

Fuselage Panel with a Window and Two Frames

This example was chosen in reference 13 to demonstrate the cross-surface interface element method. Herein, this example is solved using the cross-split method and the results from the two methods are compared. The geometry of the panel along with its displacement boundary conditions are shown in Figure 14. The fuselage panel consists of the skin and two circumferential frames. The diameter of the fuselage is 100 inches, the panel spans an arc of 34 degrees, and is 60 inches long. The skin of the panel is 0.075 inches thick with a Young's modulus of $E = 10^7$, and a Poisson's ratio of $\nu = 0.3$. The stiffeners are 0.10 inches thick with the same material properties as the skin. The window in the panel is 11 inches in radius and is filled with a material that is 0.3 inches thick, with a Young's modulus of $E = 5 \times 10^6$, and a Poisson's ratio of $\nu = 0.3$. The curved edges of the panel are clamped, while the straight edges and the free length of the frames are free in the axial (z) direction and constrained in the other directions. The finite element models for the frames were generated independently of that for the skin, and the frames may be placed at any position along the axis of the fuselage. In this example the frames are separated by a distance of 39.6 inches, and they are placed at equal distances from the edges of the panel. The resulting radial displacement contours from the cross-surface interface element method are illustrated in Figure 15a and from the cross-split method are illustrated in Figure 15b. It is observed that the two figures show an overall good agreement. However, close to the stiffeners, the results are somewhat different. In particular, it is observed that along the skin-stiffener interfaces, the cross-split method is better capable of representing the effect of the stiffeners (i.e., zero displacement) than the cross-surface interface element method. This example illustrates the potential use of the cross-split method in parametric studies of built-up structures.

Implementation of the Interface Element Methodology in MSC/NASTRAN

As demonstrated in the preceding examples, the interface elements may be used for practical global/local and substructuring problems. This is the first category of applications, known as boundary application, where the engineer creates the substructures and defines the interface between them. Another category of applications, known as interior applications, occurs in problems where the nodal incompatibilities may be created by the finite element program itself. Examples of this category include h-adaptivity and automeshing.

With h-adaptivity, regions of high error in the model are meshed with smaller elements. These smaller elements can be created by subdividing larger elements or remeshing regions of the model. If larger elements are subdivided, the subdivisions must be transitioned to the rest of the model or continued to the boundaries. The interface elements avoids this issue by allowing subdivided elements to be connected to non-subdivided elements. It also avoids another issue which occurs if regions of the model are remeshed. Then, those regions must be transitioned to the existing mesh on the rest of the model, or the entire model must be remeshed, which is compute-intensive. The interface elements allow the remeshed regions of the model to be connected to the existing regions.

With automeshers, geometrical features or user-specified mesh densities may cause difficult transition areas. Using the interface elements would enable the automesher to transition between regions of large elements and small elements, and therefore reduce the number of distorted elements that could contribute to inaccurate answers.

NASA and MSC have signed a Cooperative Agreement to implement these interface elements into MSC/NASTRAN. NASA is supplying MSC with the technology, and MSC is writing the code to incorporate the technology into MSC/NASTRAN. Both MSC and NASA will then jointly validate the resulting software.

The first phase of this project, allowing the connection of p-shell elements along a common curve, is scheduled to be included in MSC/NASTRAN V69. This will allow the boundary applications, similar to the global/local and substructuring examples in this paper, to be solved with MSC/NASTRAN. Future phases of the project will include the interior applications along a common curve and later both the boundary and interior applications for the connection of p-solid elements over a common surface.

Concluding Remarks

An interface element for analyzing plate and shell structures composed of two or more independently modeled finite element subdomains has been described and applied herein to selected global/local and substructuring examples. The approach by which the method will be implemented in MSC/NASTRAN was also described. The method allows the analyst to incorporate a detailed model of the local subdomain within the global model. The local model need not be nodally compatible with the global model. Thus, the need for tedious transition modeling is eliminated. A hybrid variational formulation was utilized to achieve compatibility, in a variational sense, between the nodally incompatible models.

In addition, a cross-split method was described for built-up structures for which the components are modeled independently and their meshes not only are nodally incompatible but the boundary nodes from one component (e.g., the stiffener) crosses the element faces of the other component (e.g., the skin).

The interface element described herein was applied to several demonstration problems. Excellent agreement is obtained between the coupled analysis solutions using the interface element and the ref-

erence solutions which are documented in the literature. The potential of the method for the detailed analysis of complicated shell structures was demonstrated by the coupled analysis of a composite laminate fuselage crown panel and a side panel with a hole and two frames.

The interface element presented herein provides a technique for predicting local and detailed stress states for plate and shell structures. The simplified modeling provided by the interface element should enhance efficiency of analysis methods and provide the modeling flexibility needed to address local details. Such enhancements should lead to a means of integrating detailed analysis into the design process.

The interface element may also be extended to dynamic and nonlinear regimes. Furthermore, the interface element may be used in conjunction with adaptive refinement techniques. In this case, the finite element domain may be subdivided into several regions and each region may be refined uniformly and independently according to some error measure. In this way the errors due to element distortion after between refinement levels is eliminated. This is in contrast to adaptive refinement techniques which usually generate badly distorted elements which in turn introduce errors due to element distortion.

NASA and MSC have signed a Cooperative Agreement to implement these interface elements into MSC/NASTRAN. The first phase of this project, allowing the connection of p-shell elements along a common curve, is scheduled to be included in MSC/NASTRAN V69. Future phases of the project will include the connection of p-solid elements over a common surface.

References

1. Schaeffer, H.G., *MSC/NASTRAN Primer, Static and Normal Modes Analysis*, Schaeffer Analysis, Inc., Mont Vernon, New Hampshire 1979, pp. 262-265.

2. Maday, Y., Mavriplis, D., and Patera, A., "Nonconforming Mortar Element Methods: Application to Spectral Discretizations," NASA CR-181729, ICASE Report No. 88-59, October, 1988.

3. Aminpour, M.A., Ransom, J.B., and McLeary, S.L., "Coupled Analysis of Independently Modeled Finite Element Subdomains," *Proceedings of the 33rd AIAA/ASME/ASCE/AHS/ASC Structures, Structural Dynamics and Materials Conference*, April 13-15, 1992, Dallas, TX, part 1, pp. 109-120, AIAA paper 92-2235.

4. Aminpour, M.A., McLeary, S.L., Ransom, J.B., and Housner J.M., "A Global/Local Analysis Method for Treating Details in Structural Design," *ASME AMD-Vol. 157, Adaptive, Multilevel, and Hierarchical Computational Strategies*, edited by A.K. Noor, pp. 119-137, 1992.

5. Ransom, J.B., McCleary, S.L., and Aminpour, M.A., "A New Interface Element for Connecting Independently Modeled Substructures," *Proceedings of the 34th AIAA/ASME/ASCE/AHS/ASC Structures, Structural Dynamics and Materials Conference*, April 19-22, 1993, La Jolla, CA, part 3, pp. 1693-1703, AIAA paper 93-1503.

6. Aminpour, M.A., Krishnamurthy, T., McCleary, S.L., and Baddourah, M.A., "Application of a New Interface Element to the Global/Local Analysis of a Boeing Composite Crown Panel," *Fourth NASA/DoD Advanced Composites Technology Conference*, June 7-11, 1993, Salt Lake City, UT, NASA CP-3229, compiled by J.G. Davis, Jr., J.E. Gardner, and M.B. Dow, Volume I, part 2, pp. 773-788, 1993.

7. Zienkiewicz, O.C., *The Finite Element Method.* Third Edition, McGraw–Hill Book Company, UK, 1977, pp. 304-328.

8. Atluri, S.N., Nishioka, T., and Nakagaki, M., "Numerical Modeling of Dynamic and Nonlinear Crack Propagation in Finite Bodies by Moving Singular Elements," *Nonlinear and Dynamic Fracture Mechanics*, (Edited by N. Perrone and S.N. Atluri, AMD), Vol. 35, ASME 1979, pp. 37-66.

9. Gunther, C.K., Holsapple, K.A., and Kobayashi, A.S., "Finite Element Analysis of Cracking Bodies," *AIAA J.* 19, 1981, pp. 789-795.

10. Aminpour, M.A., and Holsapple, K.A., "Finite Element Solutions for Propagating Interface Cracks with Singularity Elements," *Engineering Fracture Mechanics*, Vol. 39, No. 3, 1991, pp. 451-468.

11. Jinping, Z., and Huizu, S., "Stress Analysis Around Holes in Orthotropic Plates by the Subregion Mixed Finite Element Method," *Computers and Structures*, Vol. 41, No. 1, 1991, pp. 105-108.

12. BCSLIB-EXT Mathematical Library, The Boeing Extended Mathematical Subprogram Library, Copyright 1989, 20462-0520-R2 November 1991.

13. Dávila, C.G. and Aminpour, M.A., "Cross-Surface Interface Element for Coupling Built-up Structural Subdomains," *Proceedings of the 35^d AIAA/ASME/ASCE/AHS/ASC Structures, Structural Dynamics and Materials Conference,* April 18-21, 1994, Hilton Head, SC, Part 1, pp. 244-252, AIAA paper 94-1336.

14. Timoshenko, S.P., and Goodier, J.N., *Theory of Elasticity.* Third Edition, McGraw-Hill Book Company, New York, 1970, pp. 90-97.

15. Pagano, N.J., "Stress Fields in Composite Laminates," *International Journal of Solids and Structures*, Vol. 14, 1978, pp. 285-400.

16. Vidussoni, M.A., "Global-Local Finite Element Analysis of Laminated Composites, M.S. Thesis in Engineering Science and Mechanics, Virginia Polytechnic Institute and State University, July 1988.

17. Park, K.C., Stanley, G.M., "A Curved C^0 Shell Element Based on Assumed Natural-Coordinate Strains," *ASME Journal of Applied Mechanics*, Vol. 108, 1986, 278–290.

18. Dávila, C.G. and Johnson, E.R., "Delamination Initiation in the Postbuckled Dropped-Ply Laminates," Center for Composite Materials and Structures, Virginia Polytechnic Institute and State University, CCMS-91-24 (also available as VPI-E-91-23), December 1991.

19. Johnson, E.R., and Dávila, C.G., "General Purpose Solid-to-Shell Transition Elements for Geometrically Nonlinear Analysis," *Composites Engineering*, Vol. 14, 1978, pp. 285-400.

20. Minguet, P.J., Fedro, M., O'Brien, T.K., Martin, R., Ilcewicz, L., Awerbuch, J., and Wang, A., "Development of a Structural Test Configuration," *Fourth NASA/DoD Advanced Composites Technology Conference*, June 7-11, 1993, Salt Lake City, UT, NASA CP-3229, compiled by J.G. Davis, Jr., J.E. Gardner, and M.B. Dow, Volume I, part 2, pp. 863-880, 1993.

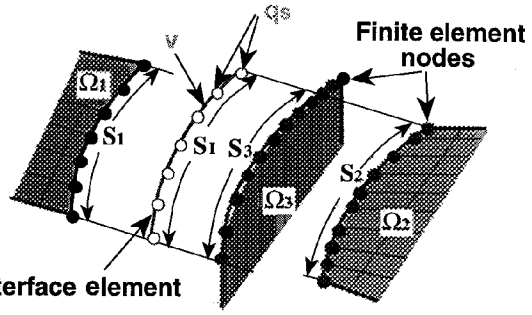

Figure 1. Interface Element Depiction.

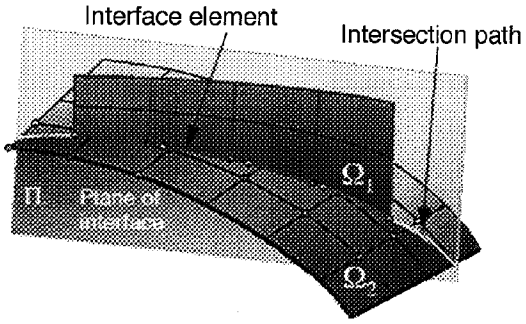

Figure 2. Cross-Surface Method.

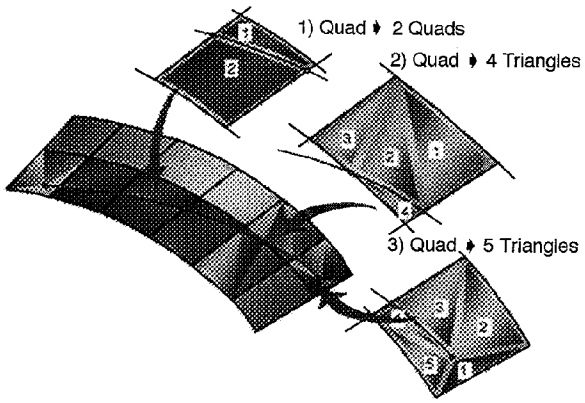

Figure 3. Cross-Split Method.

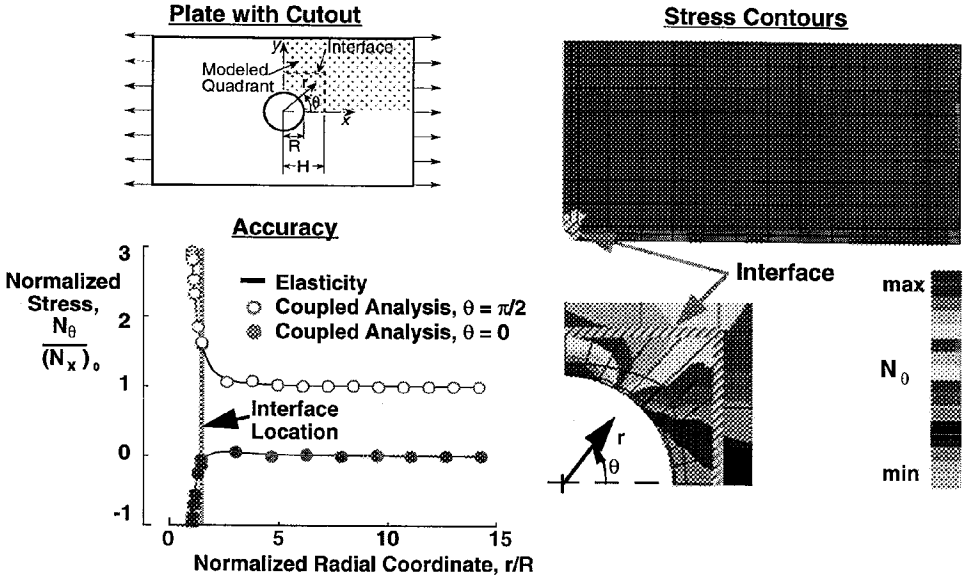

Figure 4. Accuracy of Interface Element Demonstrated on Plate Example.

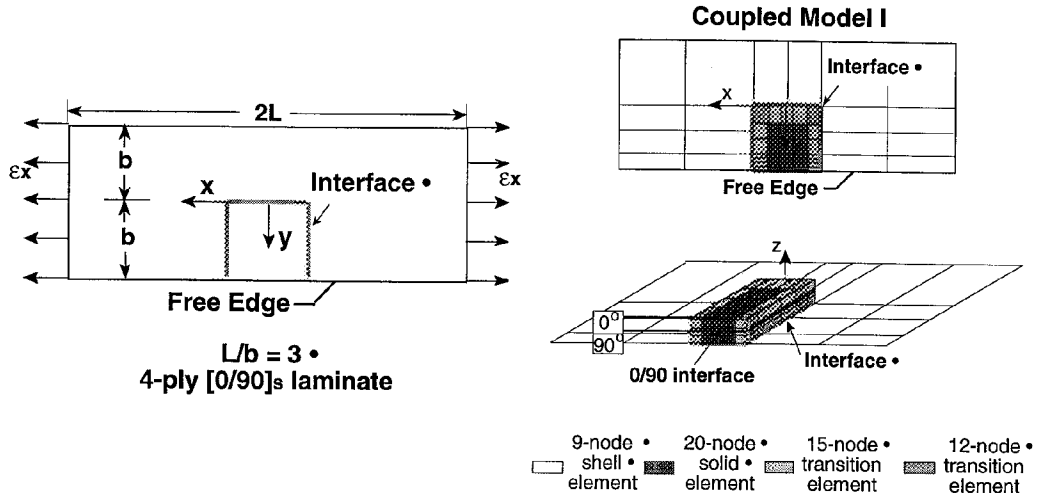

Figure 5. Tension-Loaded Composite Laminate Plate.

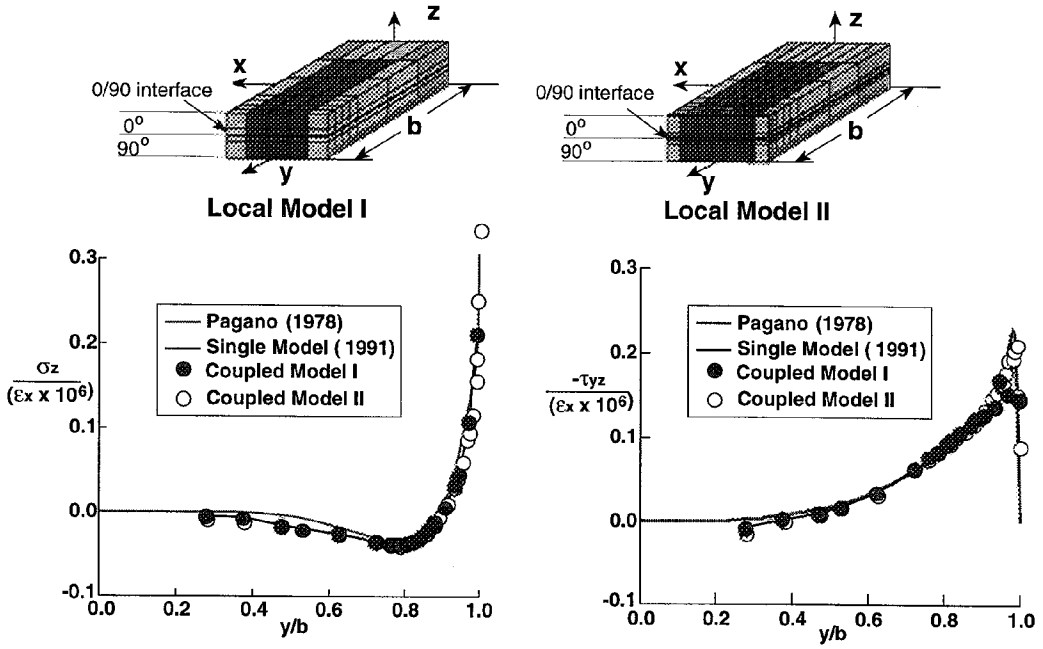

Figure 6. Interlaminar Normal and Shear Stress Distributions.

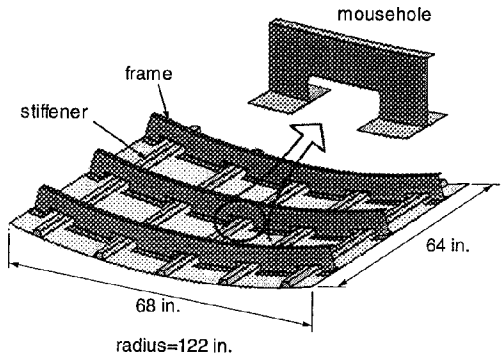

Figure 7. Composite Crown Panel.

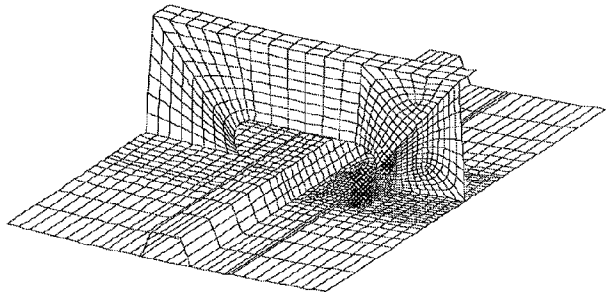

Figure 8. Transition Modeling.

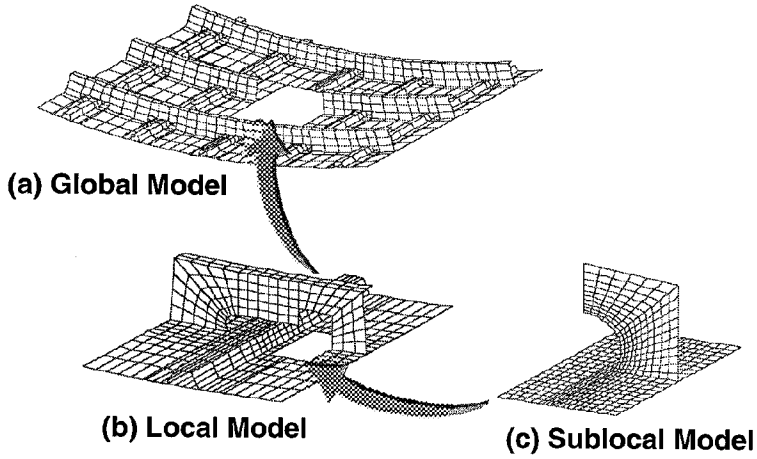

Figure 9. Nested Finite Element Models.

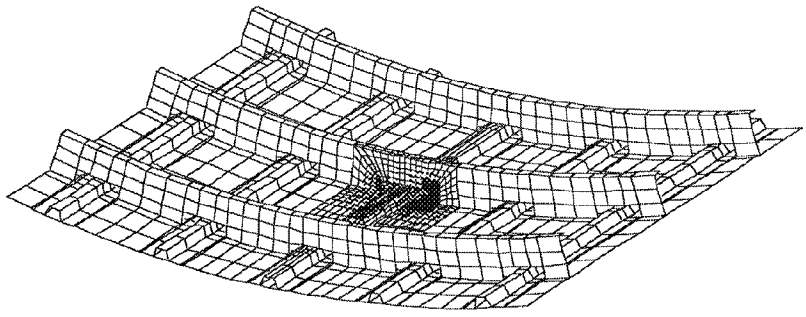

Figure 10. The Combined Finite Element Model.

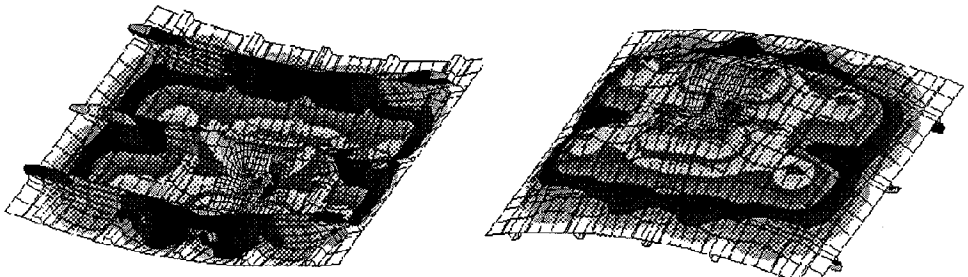

(a) Interior View (b) Exterior View

Figure 11. Deformation Contours Showing Pressure Pillowing.

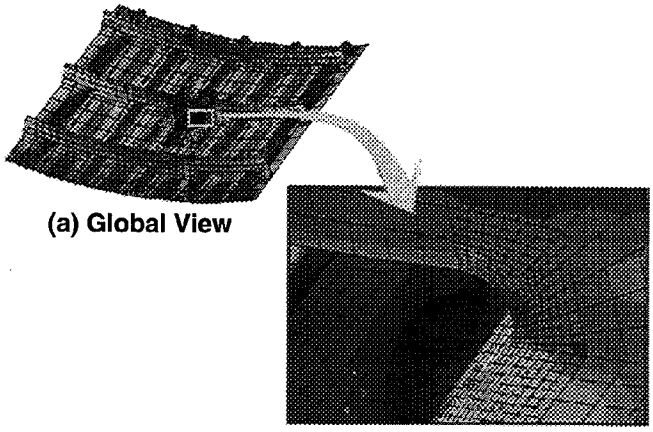

(a) Global View

(b) Local View

Figure 12. Hoop Stress Contours.

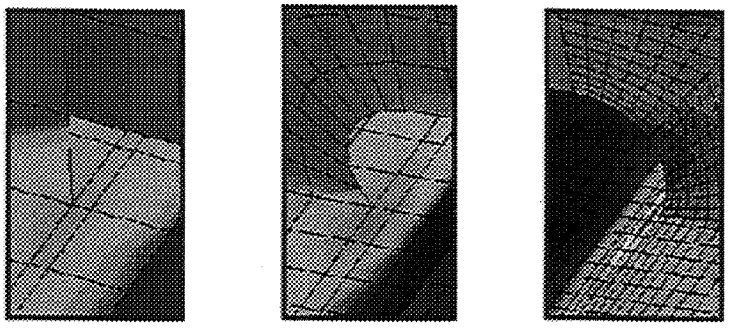

(a) Global Model of Mouse Hole (b) Local Model of Mouse Hole (c) Sublocal Model of Mouse Hole

Figure 13. Hoop Stress Comparison for Different Levels of Refinement.

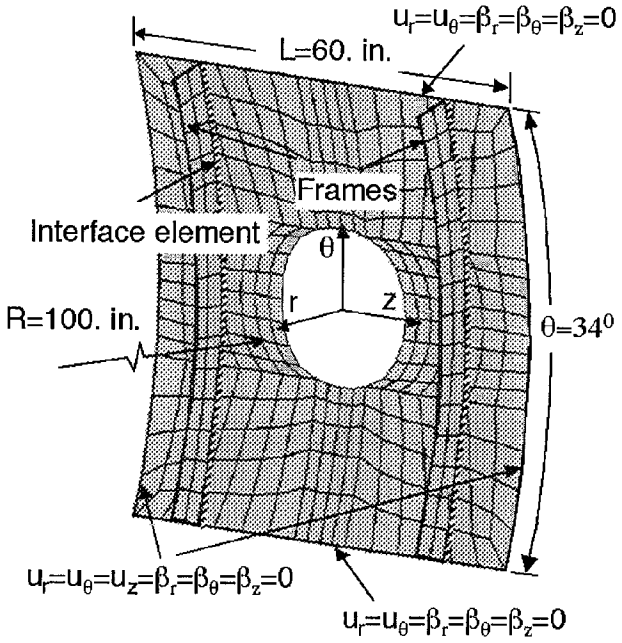

Figure 14. Model of Fuselage Panel with Window and Two Frames.

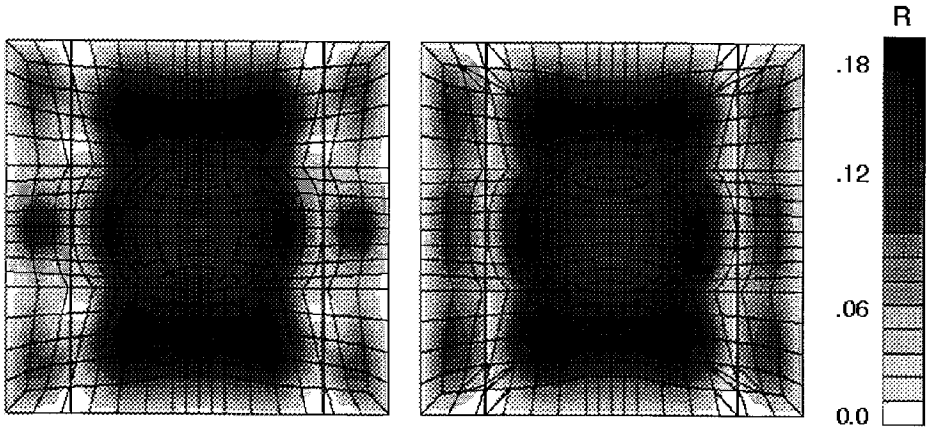

(a) Cross-Surface Method **(b) Cross-Split Method**

Figure 15. Radial Displacement Contours for Fuselage Panel.